Chemical Papers (2018) 72:1327–1337
https://doi.org/10.1007/s11696-018-0384-z

ORIGINAL PAPER

$Bi_2O_3/BiFeO_3$ heterostructure: preparation, characterization, and photocatalytic activity

Yingying Shi[1] · Ming Xiao[1] · Lijun Luo[2] · Yefei Zhang[1] · Shan Wang[1] · Yu Chen[1] · Yanju Long[1] · Lingxin Li[1] · Fengzhi Jiang[1]

Received: 20 June 2017 / Accepted: 4 January 2018 / Published online: 13 January 2018

Abstract

$Bi_2O_3/BiFeO_3$ composite was successfully fabricated by a conventional sol–gel method and structural properties were characterized based on X-ray diffractometer, scanning electron microscope, transmission electron microscope, energy-dispersive X-ray analyzer, nitrogen adsorption–desorption measurement, and UV–visible diffuse reflectance spectroscopy. $Bi_2O_3/BiFeO_3$ had a good absorption for visible light, which was benefit to photocatalytic activity. The highest degradation efficiency was obtained when the content of Bi_2O_3 in $Bi_2O_3/BiFeO_3$ was 63.9%. Effect of experimental conditions was investigated, and the highest photocatalytic activity of $Bi_2O_3/BiFeO_3$ was observed at photocatalyst dosage of 0.5 g/L, initial BPA concentration of 10 mg/L, and solution pH of 6.3. $Bi_2O_3/BiFeO_3$ photocatalyst exhibited enhanced photocatalytic activity for BPA, and the reaction rate constant over $Bi_2O_3/BiFeO_3$ composite was 2.23, 3.65, and 8.71 times higher than that of $BiFeO_3$, Bi_2O_3 and commercial TiO_2 (P25), respectively. $Bi_2O_3/BiFeO_3$ showed high photocatalytic activity after three cycles, suggesting that it was a stable photocatalyst. The possible photocatalytic mechanism has been discussed on the basis of the theoretical calculation and the experimental results. The hydroxyl and superoxide radicals together with photogenerated holes played significant roles in the photocatalytic reaction.

Keywords Bi_2O_3 · $BiFeO_3$ · Composites · Sol–gel · Photocatalysis · Bisphenol A

Introduction

Owing to its extensive usage in industry (Chen et al. 2016), bisphenol A (BPA) has been widely distributed in the environment (Falconer et al. 2006; Vom Saal and Welshons. 2014; Manfo et al. 2014). It is a kind of endocrine disrupting compounds (EDCs), which can cause adverse effects on humans and animals through the interactions with the endocrine system (Paulose et al. 2015; Jandegian et al. 2015; Li et al. 2010). BPA is stable in environment, hardly degraded and tends to bio-accumulate, which makes it very urgent and important for us to develop a sustainable, effective, and economical method to remove BPA in water.

Various methods have been developed to remove BPA from water, such as biological method (Takamiya et al. 2008), chemical oxidation method (Keykavoos et al. 2013), adsorption method (Son and Takaomi 2011), and photocatalysis method (Chen et al. 2015). Among them, the photocatalysis method is the most promising technology for the degradation of BPA because of its high degradation and mineralization efficiency, low cost, low toxicity, and its operating ability under ambient conditions. TiO_2 is a typical photocatalyst for its good chemical stability, non-toxicity, low cost, and significant photocatalytic activity (Kumar and Rao. 2017; Lin et al. 2012; Sun et al. 2016). However, pure TiO_2 absorbs only ultraviolet light which accounts for only 5% of sunlight. The rapid recombination of photogenerated

Yingying Shi and Ming Xiao two authors contributed equally to this paper.

Electronic supplementary material The online version of this article (https://doi.org/10.1007/s11696-018-0384-z) contains supplementary material, which is available to authorized users.

✉ Fengzhi Jiang
fengzhij@ynu.edu.cn

[1] School of Chemical Science and Technology, Yunnan University, Kunming 650091, China

[2] The Engineering Laboratory of Polylactic Acid-Based Functional Materials of Yunnan Province, School of Chemistry and Biotechnology, Yunnan MinZu University, Kunming 650500, China

electron–hole pairs limits the practical application of TiO_2 (Yap et al. 2010). Therefore, the study has been a hot topic for developing visible-light-driven photocatalysts. Recently, bismuth-based photocatalysts have attracted much interest because of their narrow bandgaps such as Bi_2O_3 (Yan et al. 2014a, b), Bi_2S_3 (Gao et al. 2015), Bi_2WO_6 (Kumar and Rao. 2015; Liu et al. 2015), and $BiVO_4$ (Li et al. 2015).

Bi_2O_3 is an important inorganic functional material (Yan et al. 2014a, b). It has got much attention due to its unique optical and electrical properties, which lead to its extensive usage in catalysis, optical coatings, microelectronics, solid fuel cells, gas sensors and glass manufacturing, etc. In addition, it is a good photocatalyst with a narrow bandgap ranging from 2.0 to 2.9 eV. However, there are still some problems for its practical application. The rapid recombination of photogenerated electron–hole pairs leads to the relatively low photocatalytic activity. $BiFeO_3$ is also a promising photocatalyst for its high chemical stability, narrow bandgap (2.0–2.8 eV), and special ferroelectric and ferromagnetic properties (Humayun et al. 2016; Gao et al. 2016). However, the photocatalytic activity of pure $BiFeO_3$ is not satisfying because of its low conduction band position and small surface areas (Lam et al. 2017). It is expected that the combination of Bi_2O_3 with $BiFeO_3$ would inhibit the recombination of photogenerated electron–hole pairs and enhance the photocatalytic activity.

Recently, sol–gel method was used in the synthesis of $BiFeO_3$, which has great advantages on the purity of $BiFeO_3$ and the nanoparticle morphology (Majid et al. 2015; Kim et al. 2005). In this work, the Bi_2O_3/$BiFeO_3$ composite photocatalysts were prepared by a novel sol–gel method which is rarely investigated in the literature. The Bi_2O_3/$BiFeO_3$ composite was fabricated in a single step and the content of Bi_2O_3 in the heterostructure was controlled by varying the initial molar ratio of Bi/Fe in the synthesis step. The composite photocatalyst was characterized and its photocatalytic activity for BPA was also investigated. Meanwhile, the effects of experimental conditions on the BPA degradation efficiency were discussed. A possible photocatalytic mechanism was tentatively proposed on the basis of the theoretical calculation and the experimental results.

Experimental

Preparation of the photocatalyst

All chemicals were of analytical purity and were used as received without further purification. Ultrapure water was used throughout this study. In a typical approach to obtain the composite, 7.28 g $Bi(NO_3)_3{\cdot}5H_2O$ and 2.02 g $Fe(NO_3)_3{\cdot}9H_2O$ (molar ratio of Fe/Bi = 1:3) were dissolved in 36 mL ethylene glycol in a 100 mL glass beaker under magnetic stirring, and 5 mL glacial acetic acid was added. This mixture was then heated at 80 °C for 6 h in SZCL-2 magnetic stirrer (Yuhua, China), resulting in a dark yellow sol. The sol was heated at 100 °C for 24 h in a watch-glass to get the yellow gel, and was then calcinated in a muffle furnace at 500 °C (ramping rate of furnace was 2 °C/min) for 2 h to produce Bi_2O_3/$BiFeO_3$ composite. For comparison, pure Bi_2O_3 was obtained without adding $Fe(NO_3)_3{\cdot}9H_2O$, and pure $BiFeO_3$ was obtained with an initial Fe/Bi molar ratio of 1:1 by sol–gel method.

Characterization

The crystal phases of the sample powders were characterized by TTRIII X-ray diffractometer (XRD, Rigaku, Japan) with Cu Kα radiation in the 2θ range from 10° to 80°. The surface morphology was observed on FEI QUANTA200 scanning electron microscope (SEM, USA) and JEM-2100 transmission electron microscope (TEM, JEOL, Japan). The elemental composition was analyzed using an energy-dispersive X-ray (EDAX) analyzer attached to the TEM. Nitrogen (N_2) adsorption–desorption measurement at 77 K was conducted using TriStar II 3020 (Micromeritics Inc., USA). The surface area of samples was obtained using the Brunauer–Emmett–Teller (BET) plot of N_2 adsorption isotherm. The ultraviolet–visible diffuse reflectance spectra (UV–Vis DRS) were recorded at room temperature on a UV-240IPC (JEOL, Japan) spectrophotometer using $BaSO_4$ as a reference.

Photocatalytic activity

Photocatalytic activity of the prepared photocatalysts was investigated through degradation of BPA. The photocatalysis was conducted in an XPA-7 photochemical reactor (Xujiang Electromechanical Plant, Nanjing, China). A 500 W Xe lamp and a filter ($\lambda > 420$ nm, Xujiang Electromechanical Plant, Nanjing, China) were used to get visible light. In each test, the photocatalyst was added into a quartz tube with 10.0 mL of BPA solution. Before the photocatalytic degradation experiment, the catalyst and BPA solution were mixed and stirred for 30 min in dark to reach adsorption equilibrium. Then, under the visible-light irradiation, the quartz tube was taken out at given time intervals.

BPA concentration was detected by high-performance liquid chromatography (HPLC, Agilent Technologies 1200 series) at the detection wavelength of 226.16 nm. A Symmetry C18 column (5 μm, 4.6 × 250 mm) was used as separation column. The mobile phase used for HPLC experiments was a mixture of acetonitrile and water (65/35, v/v). The flow rate was set as 1.0 mL/min, the column temperature was 35 °C, and the injection volume was 20 μL.

The degradation efficiency of BPA was calculated by the following equation:

$$\text{Degradation efficiency of BPA } (\%) = \left(C_0 - C_t\right)/C_0 \times 100\%. \quad (1)$$

C_0 and C_t represent the initial concentration of BPA before irradiation and the concentration of BPA remaining in the solution at irradiation time of t, respectively.

A pseudo-first-order kinetic model was used to evaluate the photodegradation efficiency and the degradation kinetics constant k was obtained as

$$\ln\left(C_t/C_0\right) = -kt. \quad (2)$$

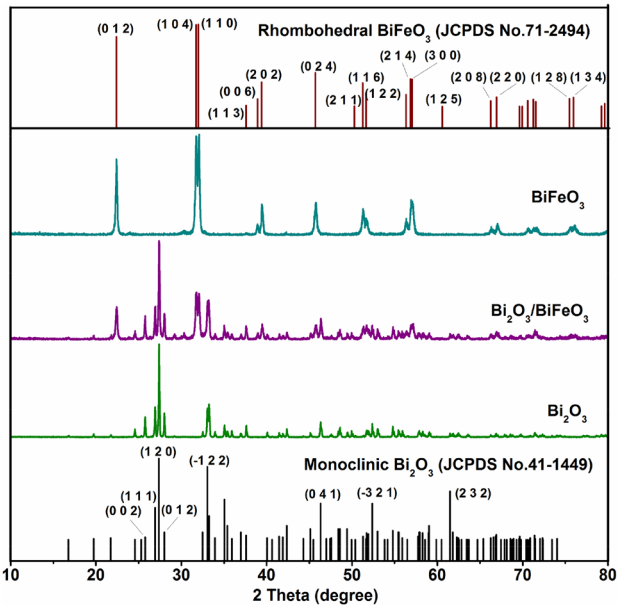

Fig. 1 XRD pattern of single phase and composite photocatalysts

Results and discussion

Characterization

XRD analysis

The chemical composition and phase structure of the fabricated samples were confirmed with powder X-ray diffraction (XRD). As shown in Fig. 1, all diffraction peaks of the samples could be unambiguously assigned to rhombohedral phase $BiFeO_3$ (JCPDS No. 71-2494) (Fan et al. 2015) and monoclinic Bi_2O_3 (JCPDS No. 41-1449) (Cheng and Kang 2014), respectively. The sharp diffraction peaks indicated that the samples were well crystallized. No impurity peaks were observed, indicating a high purity of the products. The $Bi_2O_3/BiFeO_3$ composite exhibited a co-existence of both Bi_2O_3 and $BiFeO_3$ phases without significant change in the peak positions, indicating that the combination of the two materials did not change the crystal structure of Bi_2O_3 and $BiFeO_3$.

SEM analysis

The morphologies and surface structures of fabricated samples were studied by SEM. Figure 2a displays the morphology of pure $BiFeO_3$. Pure $BiFeO_3$ was composed of spherical nanoparticles. The particle size was relatively uniform, and some particles were contacted with each other. The morphology of pure Bi_2O_3 is shown in Fig. 2b. Pure Bi_2O_3 displayed mainly nanosheet shape with a thickness in 40–65 nm. From Fig. 2c, it was clearly seen that Bi_2O_3 nanosheets were surrounded by lots of $BiFeO_3$ nanoparticles, indicating that the two materials were well integrated at the structural level.

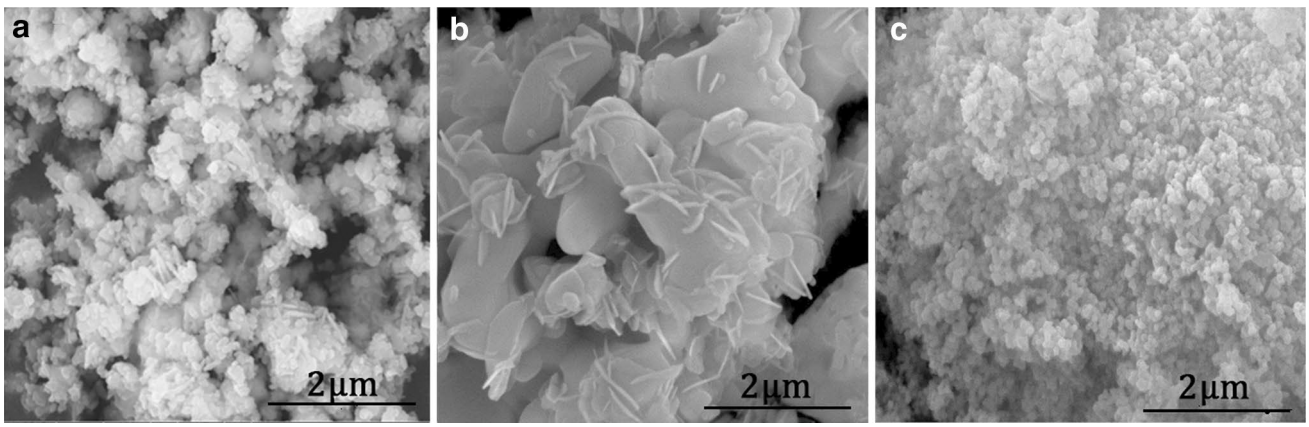

Fig. 2 SEM images of $BiFeO_3$ (**a**), Bi_2O_3 (**b**), and $Bi_2O_3/BiFeO_3$ (**c**)

TEM and EDS analysis

The morphologies of photocatalysts were further studied by TEM. The TEM image shown in Fig. 4a confirmed that the structure of individual $BiFeO_3$ was nanoparticles. The diameter of the spherical particles was 50–100 nm. Figure 4b shows that the structure of individual Bi_2O_3 was nanosheets. Figure 4c, d shows that the Bi_2O_3/$BiFeO_3$ composite was formed from the combination of Bi_2O_3 nanosheets with $BiFeO_3$ nanoparticles. Moreover, the element composition of the fabricated Bi_2O_3/$BiFeO_3$ composite was determined by energy-dispersive X-ray spectroscopy (EDS). Figure 3e, f shows taken from the corresponding EDS spectrum of rectangular region A from a nanosheet and region B from a nanoparticle in Fig. 3c, respectively. The Cu-element interference peaks shown in Fig. 3e, f were from the copper mesh which was used as the base. The spectrum showed characteristic peaks of Bi and O in Fig. 3e, while the peaks corresponded to Bi, O, and Fe elements can be detected in Fig. 3f. The peaks further indicated that the nanosheets were consisted of Bi_2O_3 and nanoparticles of $BiFeO_3$ and the Bi_2O_3/$BiFeO_3$ composite indeed formed from the two materials.

BET analysis

Figure 4 shows the N_2 adsorption–desorption isotherms of Bi_2O_3/$BiFeO_3$, Bi_2O_3, and $BiFeO_3$. The isotherm of Bi_2O_3/$BiFeO_3$ was belong to type V with an H3 hysteresis loop, indicating that the composite exhibited a porous structure and the slit pores were formed by the accumulation of nanosheets and nanoparticles. Such porous structure was extremely useful in photocatalysis as it would provide communicable channels for the diffusion of reactant molecules and products. The BET-specific surface area of Bi_2O_3/$BiFeO_3$ was observed as 4.98 m^2/g, while the BET surface areas of Bi_2O_3 and $BiFeO_3$ were estimated to be 2.15 and 9.09 m^2/g, respectively. The result showed that a large specific surface area was not essential for the high performance of composite in the present study.

UV–Vis DRS analysis

The UV–Vis diffuse reflectance spectra (DRS) of the samples were investigated with the aim to probing their optical properties. As shown in Fig. 5a, commercial TiO_2 (P25) absorbed only ultraviolet light ($\lambda < 420$ nm). Pure Bi_2O_3 and $BiFeO_3$ showed absorption edges at about 455 and 570 nm, respectively, indicating that Bi_2O_3 and $BiFeO_3$ could absorb light with wavelength from UV to visible regions. Bi_2O_3 has stronger absorbance in UV region, while $BiFeO_3$ in visible region. Bi_2O_3/$BiFeO_3$ composite had an absorption edge at about 560 nm, which was between the absorption edge of Bi_2O_3 and $BiFeO_3$.

The optical absorption performance of a semiconductor is evaluated based on band-gap energy (E_g). The band-gap energy (E_g) was evaluated using the following equation (Xiao et al. 2013):

$$\alpha h\nu = k\left(h\nu - E_g\right)^{n/2}. \tag{3}$$

In this equation, α, h, ν, k, and E_g represent absorption coefficient, Planck constant, light frequency, a constant, and band-gap energy, respectively. In addition, the absorbance (A) of the photocatalyst is proportional to its absorption coefficient (α). The value of n depends on the characteristic of the transition in a semiconductor; it is 1 for Bi_2O_3 and 4 for $BiFeO_3$ (Xiao et al. 2013; Tong et al. 2016). The band-gap energy of $BiFeO_3$ was calculated to be 1.70 eV, and the band-gap energy of Bi_2O_3 was 2.83 eV.

The conduction band (CB) and valence band (VB) positions of Bi_2O_3 and $BiFeO_3$ were speculated by a theoretical method. The CB (E_{CB}) and VB (E_{VB}) positions of a semiconductor can be calculated by the following equations (Feng et al. 2015):

$$E_{VB} = X - E_e + 0.5E_g, \tag{4}$$

$$E_{CB} = E_{VB} - E_g, \tag{5}$$

where X is the absolute electronegativity of the semiconductor. E_e is the energy of free electrons on the hydrogen scale (about 4.5 eV). E_g is the band-gap energy of the semiconductor. The results are shown in Table 1.

Effect of initial Fe/Bi molar ratio

To investigate the effect of the initial Fe/Bi molar ratio, a series of Bi_2O_3/$BiFeO_3$ samples with different initial Fe/Bi molar ratios (1:1, 1:2, 1:3, and 1:4) were fabricated. The XRD patterns of the samples are shown in Fig. S1. When the initial Fe/Bi molar ratio was 1:1, pure $BiFeO_3$ was fabricated. In addition, when the initial Fe/Bi molar ratio was 1:2, 1:3, and 1:4, monoclinic Bi_2O_3 was produced and the diffraction peaks of Bi_2O_3 gradually increased in intensity when decreasing the initial molar ratio of Fe/Bi. The mass fraction of Bi_2O_3 in Bi_2O_3/$BiFeO_3$ composites was calculated by MDI Jade 6.0 software and the results are shown in Table 2.

It was shown that the theoretical content of Bi_2O_3 and the actual content of Bi_2O_3 could be regarded as the same when increasing the initial molar ratio of Fe/Bi to 1:2. Excess Bi_2O_3 was obtained when the initial molar ratio of Fe/Bi was low. We can get the required composition according to the theoretical arithmetic and experimental results.

Figure S2 illustrates the time courses of BPA degradation efficiency over Bi_2O_3/$BiFeO_3$ composites with different initial Fe/Bi molar ratios. The degradation efficiency increased

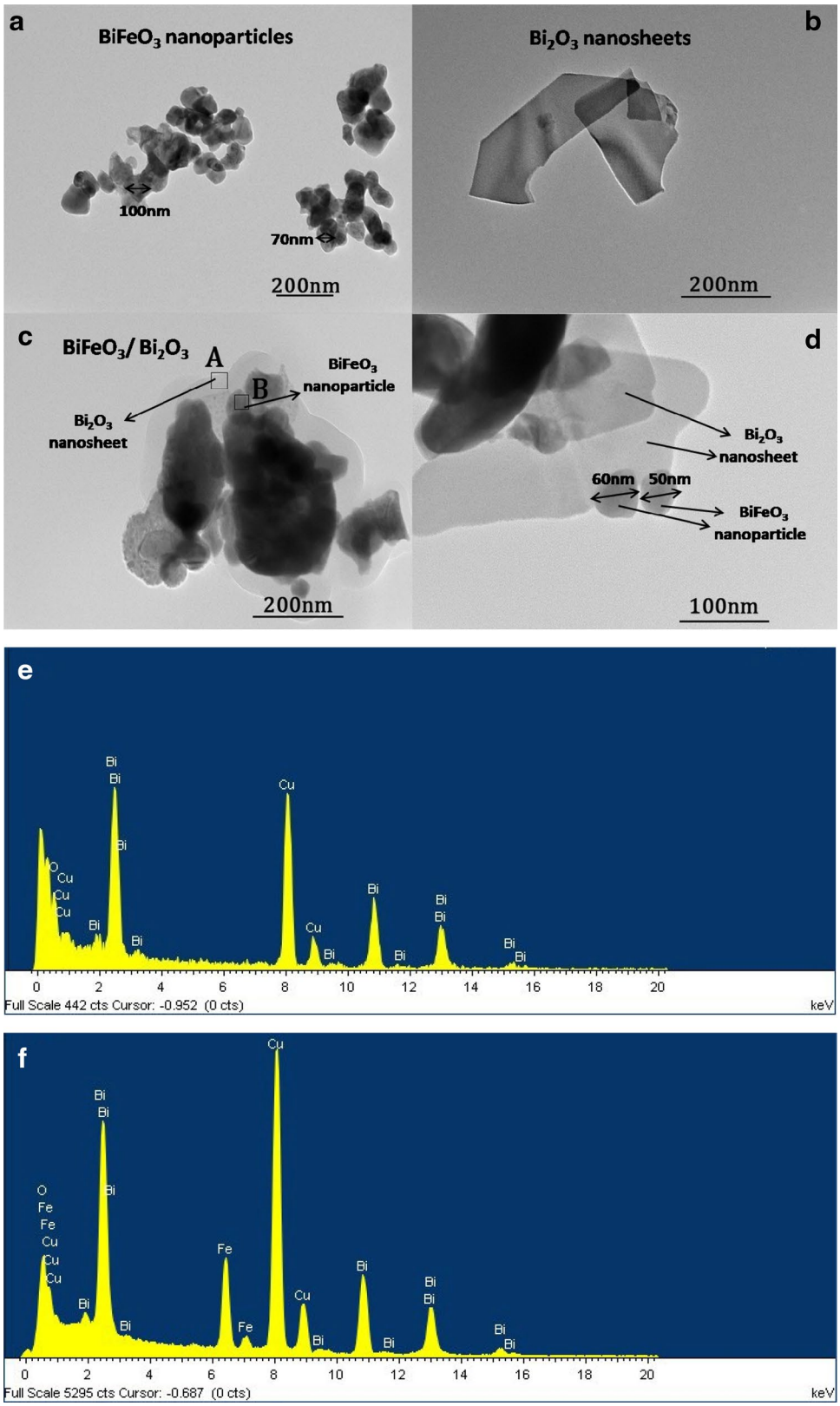

Fig. 3 TEM images of $BiFeO_3$ (**a**), Bi_2O_3 (**b**) and Bi_2O_3/$BiFeO_3$ (**c**, **d**), and the corresponding EDS spectrum of Bi_2O_3 (**e**) and $BiFeO_3$ (**f**)

from 69.8 to 86.5% after 300 min of visible-light irradiation when the initial molar ratio of Fe/Bi decreased from 1:1 to 1:3. However, when further decreased the initial Fe/Bi molar ratio in Bi_2O_3/$BiFeO_3$ composites from 1:3 to 1:4, the degradation efficiency of BPA decreased to 70.6%. The highest degradation efficiency was obtained when the content

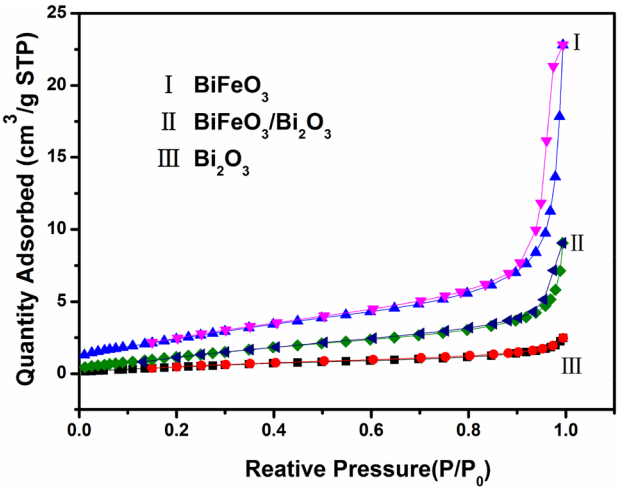

Fig. 4 Nitrogen adsorption–desorption isotherm of $BiFeO_3$, Bi_2O_3/$BiFeO_3$, and Bi_2O_3

of Bi_2O_3 in Bi_2O_3/$BiFeO_3$ was 63.9%. This result implied that a suitable content of Bi_2O_3 would help to enhance the photocatalytic activity, and the optimal initial Fe/Bi molar ratio was 1:3.

Photocatalytic degradation of BPA

Effect of photocatalyst dosage

To investigate the effect of photocatalyst dosages on the photocatalytic degradation efficiencies of BPA, various photocatalyst dosages (0.2, 0.5, 0.8, and 1.0 g/L) were used on the degradation efficiency of BPA at the initial BPA concentration of 10 mg/L, irradiation time of 300 min, and solution pH of 6.3. The results are provided in Fig. 6. The photocatalytic degradation efficiency enhanced from 57.1 to 100% in 300 min when increasing of catalyst dosage from 0.2 to 0.5 g/L. With increasing the catalyst dosage to 0.8 g/L, the degradation efficiency was still 100% after 300 min of visible-light irradiation. Further increasing the catalyst dosage to 1.0 g/L, the degradation efficiency decreased weakly to 97.4%. It was reported that lower catalytic activity was observed when a smaller amount of catalyst was used, because that insufficient catalytic active sites were applied (Chang et al. 2010). However, if the photocatalyst dosage is too high, the light penetration decreased and light scattering effect occurred (Sood et al. 2015). In addition, the number of catalytic surface active sites would decrease, which was possibly caused by the agglomeration and sedimentation of the photocatalyst particles at too high dosage (Puangpetch et al. 2010). Therefore, 0.5 g/L catalyst dosage was selected as the optimal dosage of photocatalysts for the sequential experiment.

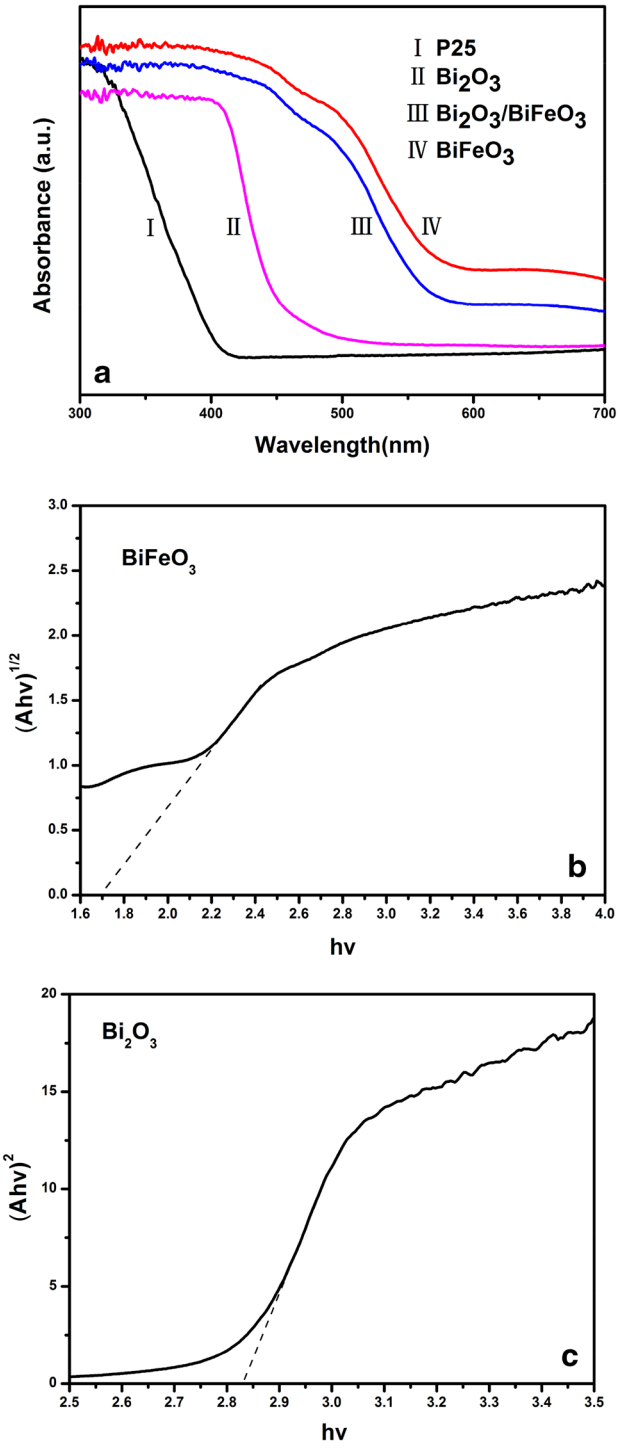

Fig. 5 UV–visible absorption spectra and Kubelka–Munk plot of various photocatalysts

Effect of initial BPA concentration

To investigate the effect of the initial BPA concentration on the photocatalytic degradation efficiencies of BPA, various initial BPA concentrations (10, 15, 20, and 30 mg/L) were

Table 1 Absolute electronegativity, calculated CB position, calculated VB position and band-gap energy for Bi_2O_3 and $BiFeO_3$

Semiconductors	Absolute electronegativity X (eV)	Calculated CB position E_{CB} (eV)	Calculated VB position E_{VB} (eV)	Band-gap energy E_g (eV)
Bi_2O_3	5.95	0.04	2.87	2.83
$BiFeO_3$	5.74	0.39	2.09	1.70

used on the degradation efficiency of BPA at catalyst dosage of 0.5 g/L, solution pH of 6.3, and irradiation time of 300 min. Results are provided in Fig. 7. The results showed that the degradation efficiencies decreased with the increase of BPA concentration. With the initial BPA concentration 10, 15, 20, and 30 mg/L, the photocatalytic degradation efficiencies at 300 min were 100, 72.0, 62.6, and 39.9%, respectively. Similar results had been reported by others using different catalysts (Chang et al. 2010). With the BPA concentration ranged from 10 to 30 mg/L, organic pollutant molecules accumulated on the surface of photocatalyst and the active sites were covered by high concentration of BPA, which resulted in the decrease of photocatalytic degradation efficiencies. Another possible reason was that more degradation intermediates were produced at higher BPA concentration, which would lead to the competitive adsorption between degradation intermediates and target pollutant (BPA), and finally caused the decrease of degradation efficiencies.

Effect of solution pH

To investigate the effect of solution pH on the degradation of BPA, BPA degradation experiments were performed in the pH range of 3.0–11.0 with catalyst dosage of 0.5 g/L, initial BPA concentration of 10 mg/L, and irradiation time of 300 min. The pH value of BPA solution in natural condition was 6.3. In addition, the other pH values were adjusted by NaOH (0.01 mol/L) and HCl (0.01 mol/L) solution. From Fig. 8, we could see that the highest degradation efficiency was obtained at natural condition (pH 6.3), and all BPA were degraded after 300 min of visible-light irradiation. The photocatalytic degradation efficiencies at solution pH of 3.0, 5.0, 7.0, 9.0, and 11.0 were 15.2, 72.3, 84.2, 59.8, and 40.4% in 300 min, respectively. It could be seen that lower photocatalytic activities were observed with the pH value deviated from natural condition. As well known, hydroxyl radicals (·OH) were generated by oxidizing hydroxide ions and they

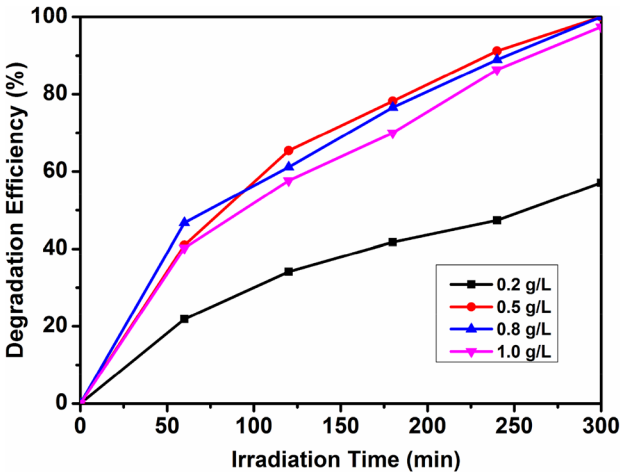

Fig. 6 Time courses of BPA degradation efficiency with different Bi_2O_3/$BiFeO_3$ photocatalyst dosages

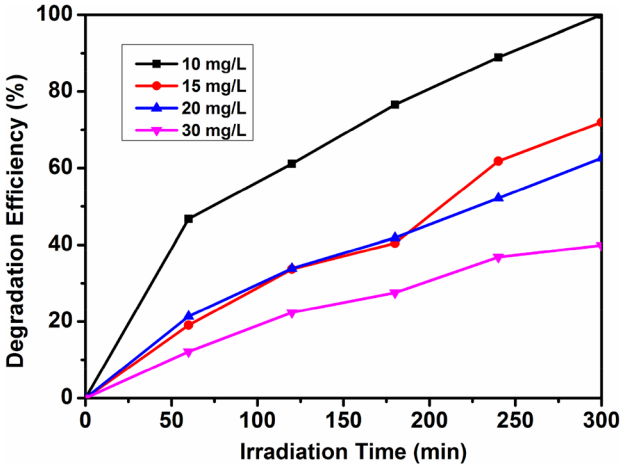

Fig. 7 Time courses of BPA degradation efficiency over Bi_2O_3/$BiFeO_3$ composite with different initial BPA concentrations

could react with much organic pollutants. It was reported that ·OH was easier to be generated by oxidizing more hydroxide ions available on photocatalyst surface in alkaline solutions (Konstantinou and Albanis 2004). Therefore, the possible cause induced low degradation efficiencies at strong acid conditions was that less hydroxyl radicals (·OH) were generated because of lower OH^- concentration, which would greatly effect the photocatalytic activities. On the other hand, BPA existed in the form of anions at alkaline condition, which may

Table 2 Effect of initial Fe/Bi molar ratio

Initial molar ratios of Fe/Bi	Fe/Bi = 1:1	Fe/Bi = 1:2	Fe/Bi = 1:3	Fe/Bi = 1:4
Composition	$BiFeO_3$	Bi_2O_3/$BiFeO_3$	Bi_2O_3/$BiFeO_3$	Bi_2O_3/$BiFeO_3$
Theoretical content of Bi_2O_3 (wt %)	0	42.7	59.8	69.1
Actual content of Bi_2O_3 (wt %)	0	42.7	63.9	89.2

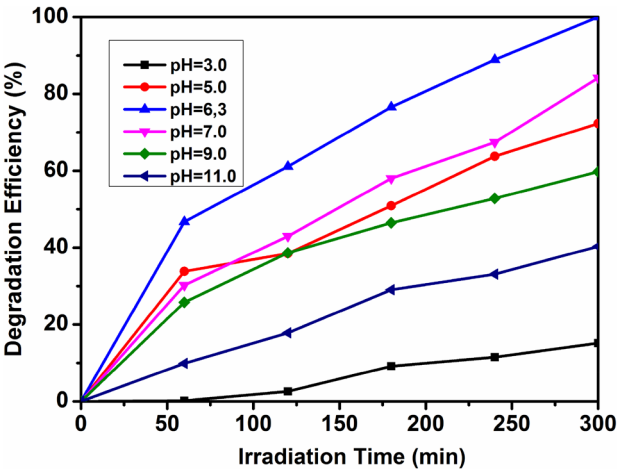

Fig. 8 Time courses of BPA degradation efficiency over Bi_2O_3/$BiFeO_3$ composite with different solution pHs

repel the negative charged surface of photocatalyst (Konstantinou and Albanis 2004) and hydroxyl radicals (·OH). And then, the photodegradation efficiencies decreased. The results indicated that the degradation efficiency of BPA over Bi_2O_3/$BiFeO_3$ composite was most favorable at natural condition.

Photocatalytic activity evaluation

To evaluate the photocatalytic activity towards BPA of prepared Bi_2O_3/$BiFeO_3$ composite, a series of experiments were carried out at photocatalyst dosage of 0.5 g/L, initial BPA concentration of 10 mg/L, irradiation time of 300 min, and solution pH of 6.3. The visible-light-driven photocatalytic properties of fabricated Bi_2O_3/$BiFeO_3$ composite, Bi_2O_3, $BiFeO_3$, and P25 are shown in Fig. 9a. Under visible-light irradiation, the self-degradation of BPA could be negligible. Bi_2O_3/$BiFeO_3$ composite showed an enhanced photocatalytic activity compared to Bi_2O_3 and $BiFeO_3$. For instance, the degradation efficiency of the Bi_2O_3/$BiFeO_3$ composite could reach nearly 100% within 300 min, while 49.2, 69.9, and 22.3% of degradation efficiencies were obtained for pure Bi_2O_3, pure $BiFeO_3$, and P25, respectively. The result indicated that the combination of Bi_2O_3 and $BiFeO_3$ could inhibit the recombination of photogenerated electron–hole pairs and enhance the photocatalytic activity efficiently.

To further investigate the photocatalysis, the degradation kinetics of BPA using fabricated Bi_2O_3/$BiFeO_3$ composite, Bi_2O_3, $BiFeO_3$, and P25 were investigated by fitting the experimental data to the pseudo-first-order kinetic model. The results shown in Fig. 9b illustrated that the reaction kinetics of all samples can be very well fitted by the pseudo-first-order rate model. The *k* value of BPA self-degradation was 0.0000673 / min, which could be neglected. In addition, the calculated k values for fabricated Bi_2O_3/$BiFeO_3$ composite, Bi_2O_3, $BiFeO_3$,

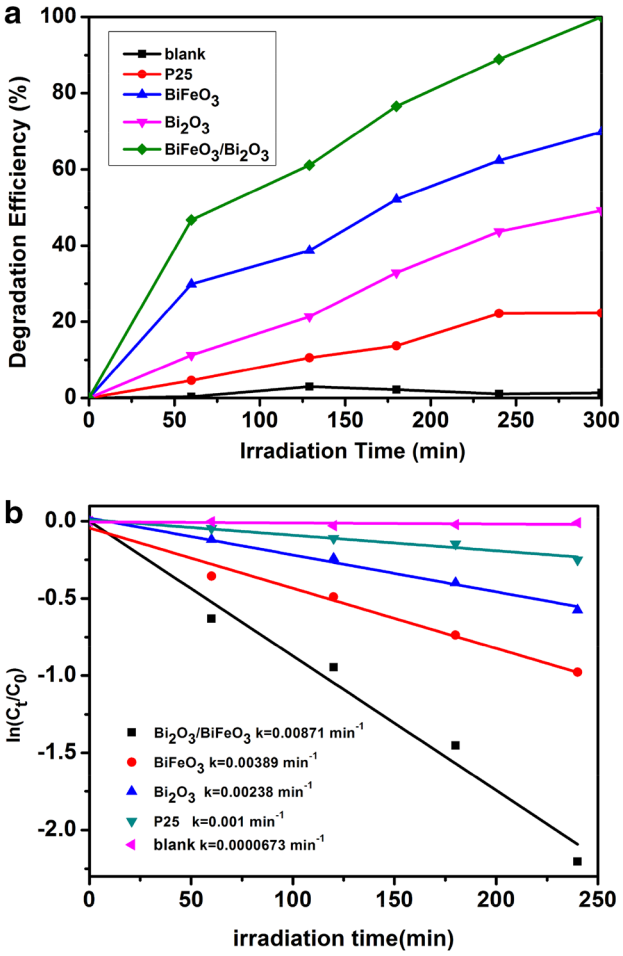

Fig. 9 Time courses of BPA degradation efficiency over Bi_2O_3/$BiFeO_3$ composite, Bi_2O_3, $BiFeO_3$ and P25 (**a**) and the corresponding fitted plots of pseudo-first-order kinetics (**b**) (experimental conditions: photocatalyst dosages of 0.5 g/L, initial BPA concentration of 10 mg/L, solution pH of 6.3, and irradiation time of 300 min)

and P25 were 0.00871, 0.00238, 0.00389, and 0.001 /min, respectively. Namely, the reaction rate constant over fabricated Bi_2O_3/$BiFeO_3$ composite is 2.23, 3.65, and 8.71 times higher than that of $BiFeO_3$, Bi_2O_3, and P25, respectively, proving that Bi_2O_3/$BiFeO_3$ composite was a promising photocatalyst.

Recyclability

To investigate the recyclability of Bi_2O_3/$BiFeO_3$ photocatalyst, the recycled experiments were carried out. After each photocatalytic reaction, the Bi_2O_3/$BiFeO_3$ photocatalyst was centrifugated and washed by anhydrous alcohol for reuse, and then, the next cycle was started with the photocatalyst dosage of 0.5 g/L, initial BPA concentration of 10 mg/L, solution pH of 6.3, and irradiation time of 300 min. From Fig. 10, the removal rate decreased from 96.9 to 71.4% after three cycles, but it is clearly shown

that the photocatalytic activity of Bi_2O_3/$BiFeO_3$ was still higher than Bi_2O_3 or $BiFeO_3$, suggesting that Bi_2O_3/$BiFeO_3$ was a stable and efficient photocatalyst.

Photocatalytic mechanism

On the basis of experimental results, a possible photocatalytic mechanism was proposed for the photodegradation of BPA over Bi_2O_3/$BiFeO_3$ composite (Fig. 11).

When Bi_2O_3/$BiFeO_3$ photocatalyst was subjected to the visible-light irradiation, both Bi_2O_3 and $BiFeO_3$ were excited with photogenerated electrons and holes produced. The photogenerated electrons in the CB of Bi_2O_3 would transfer to CB of $BiFeO_3$, and the holes in the VB of Bi_2O_3 would transfer to VB of $BiFeO_3$. This could help to reduce the recombination of electron–hole pairs, and thus, the photocatalytic activity of Bi_2O_3/$BiFeO_3$ composite could be enhanced. It was known that the standard redox potentials of $O_2/{\cdot}O_2^-$ and $\cdot OH/H_2O$ were + 0.13 and + 2.68 eV at pH 7, respectively (Chen et al. 2015). In this system, the CB edge of Bi_2O_3 was more negative than + 0.13 eV, indicating that ${\cdot}O_2^-$ radicals could be produced. In addition, the VB edge of Bi_2O_3 was more positive than + 2.68 eV, indicating that the photogenerated holes in the VB of Bi_2O_3 had enough ability to oxidize H_2O to give ·OH radicals. According to the above results, ·OH and ${\cdot}O_2^-$ radicals were produced in the process and then participated in the photocatalytic reaction. Besides, organic pollutants would be oxidized via the excess of holes in the valence band of Bi_2O_3 and $BiFeO_3$. In a word, ·OH radicals, ${\cdot}O_2^-$ radicals, and holes simultaneously participated in the degradation mechanism.

The possible reactions in the photodegradation process of BPA were as follows:

$$Bi_2O_3 \rightarrow Bi_2O_3(e^-) + Bi_2O_3\left(h^+\right)(h\nu)$$
$$BiFeO_3 \rightarrow BiFeO_3(e^-) + BiFeO_3\left(h^+\right)(h\nu)$$
$$Bi_2O_3\left(h^+\right) + H_2O \rightarrow {\cdot}OH$$
$$Bi_2O_3(e^-) + O_2 \rightarrow {\cdot}O_2^-$$
$${\cdot}O_2^- + \text{BPA} \rightarrow \text{Degradation products}$$
$${\cdot}OH + \text{BPA} \rightarrow \text{Degradation products}$$
$$Bi_2O_3\left(h^+\right) + \text{BPA} \rightarrow \text{Degradation products}$$
$$BiFeO_3\left(h^+\right) + \text{BPA} \rightarrow \text{Degradation products.}$$

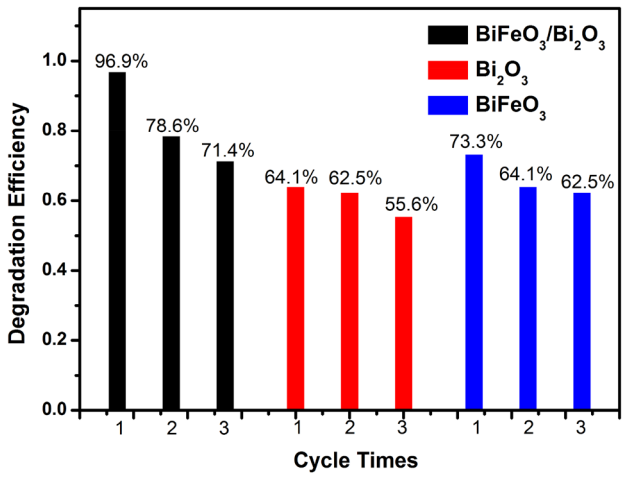

Fig. 10 Recycled photodegradation of BPA over Bi_2O_3/$BiFeO_3$, Bi_2O_3, and $BiFeO_3$ (experimental conditions: photocatalyst dosages of 0.5 g/L, initial BPA concentration of 10 mg/L, solution pH of 6.3, and irradiation time of 300 min)

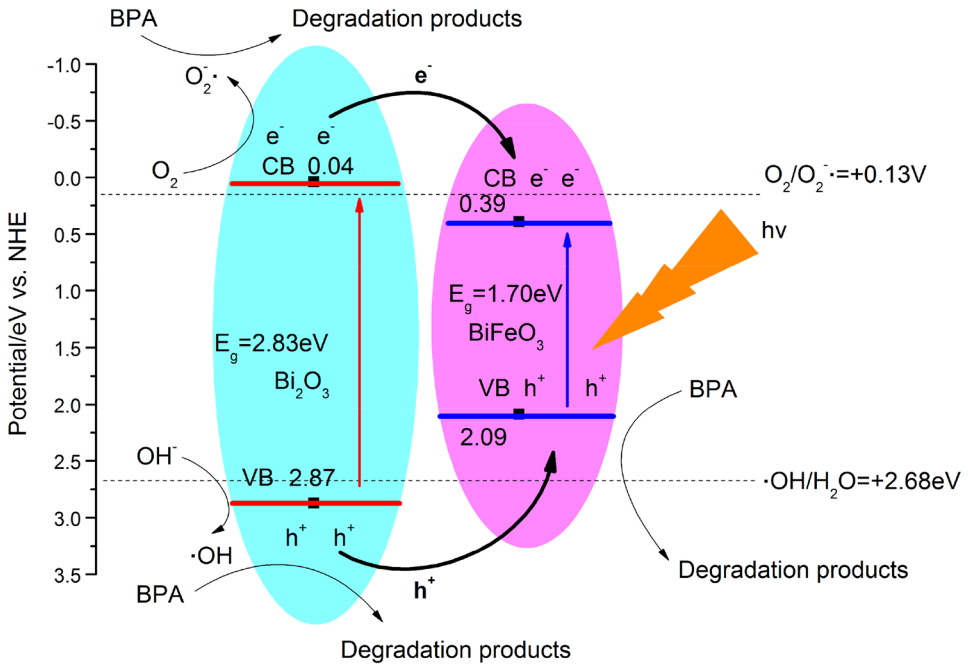

Fig. 11 Charge carrier dynamics and pollutant degradation mechanism in Bi_2O_3/$BiFeO_3$ composite under visible light

Conclusions

In this paper, $Bi_2O_3/BiFeO_3$ composite photocatalyst was successfully fabricated by a one-step sol–gel method using $Bi(NO_3)_3{\cdot}5H_2O$ as bismuth source and $Fe(NO_3)_3{\cdot}9H_2O$ as iron source. Effect of various reaction parameters on the BPA degradation under visible light was investigated in detail and concluded that the catalyst dosage of 0.5 g/L, initial BPA concentration of 10 mg/L, solution pH 6.3, and 63.9% of Bi_2O_3 in the composite was favorable to achieve maximum efficiency. The reaction rate constant over optimized $Bi_2O_3/BiFeO_3$ composite is 2.23, 3.65, and 8.71 times higher than that of $BiFeO_3$, Bi_2O_3, and P25, respectively. $Bi_2O_3/BiFeO_3$ showed high photocatalytic activity after three cycles, suggesting that it was a stable photocatalyst. According to the theoretical calculation and the experimental results, ·OH radicals, $\cdot O_2^-$ radicals, and valence band holes played significant roles in the photocatalytic reaction.

Acknowledgements This work was jointly supported by the National Natural Science Foundation of China (Nos. 21163023 and 21261026) and Key Program of Yunnan Province Foundation (No. 2013FA005).

References

Chang X, Huang J, Cheng C, Sha W, Li X, Ji G, Deng S, Yu G (2010) Photocatalytic decomposition of 4-*t*-octylphenol over $NaBiO_3$ driven by visible light: catalytic kinetics and corrosion products characterization. J Hazard Mater 173:765–772. https://doi.org/10.1016/j.jhazmat.2009.08.148

Chen Y, Tian G, Shi Y, Xiao Y, Fu H (2015) Hierarchical MoS_2/Bi_2MoO_6 composites with synergistic effect for enhanced visible photocatalytic activity. Appl Catal B Environ 164:40–47. https://doi.org/10.1016/j.apcatb.2014.08.036

Chen WY, Shen YP, Chen SC (2016) Assessing bisphenol A (BPA) exposure risk from long-term dietary intakes in Taiwan. Sci Total Environ 543:140–146. https://doi.org/10.1016/j.scitotenv.2015.11.029

Cheng L, Kang Y (2014) Selective preparation of Bi_2O_3 visible light-driven photocatalyst by dispersant and calcination. J Alloys Compd 585:85–93. https://doi.org/10.1016/j.jallcom.2013.08.010

Falconer IR, Chapman HF, Moore MR, Ranmuthugala G (2006) Endocrine-disrupting compounds: a review of their challenge to sustainable and safe water supply and water reuse. Environ Toxicol 21:181–191. https://doi.org/10.1002/tox.20172

Fan Y, Chen C, Tang Z, Ni Y, Lu C (2015) Synthesis and characterization of $g\text{-}C_3N_4/BiFeO_3$ composites with an enhanced visible light photocatalytic activity. Mater Sci Semicond Process 40:439–445. https://doi.org/10.1016/j.mssp.2015.06.054

Feng Y, Yan X, Liu C, Hong Y, Zhu L, Zhou M, Shi W (2015) Hydrothermal synthesis of CdS/Bi_2MoO_6 heterojunction photocatalysts with excellent visible-light-driven photocatalytic performance. Appl Surf Sci 353:87–94. https://doi.org/10.1016/j.apsusc.2015.06.061

Gao X, Wang Z, Fu F, Li X, Li W (2015) 2D double-layer-tube-shaped structure Bi_2S_3/ZnS heterojunction with enhanced photocatalytic activities. Physica B 474:81–89. https://doi.org/10.1016/j.physb.2015.06.002

Gao X, Dai Y, Fu F, Hua X (2016) 2D laminated cylinder-like $BiFeO_3$ composites: hydrothermal preparation, formation mechanism, and photocatalytic properties. Solid State Sci 62:6–12. https://doi.org/10.1016/j.solidstatesciences.2016.10.014

Humayun M, Zada A, Li Z, Xie M, Zhang X, Qu Y, Raziq F, Jing L (2016) Enhanced visible-light activities of porous $BiFeO_3$ by coupling with nanocrystalline TiO_2 and mechanism. Appl Catal B: Environ 180:219–226. https://doi.org/10.1016/j.apcatb.2015.06.035

Jandegian CM, Deem S, Bhandari R, Holliday CM, Nicks D, Rosenfeld CS, Selcer KW, Tillitt DE, Vom Saal F, Velez-Rivera V, Yang Y, Holliday DK (2015) Developmental exposure to bisphenol A (BPA) alters sexual differentiation in painted turtles (Chrysemys picta). Gen Comp Endocrinol 216:77–85. https://doi.org/10.1016/j.ygcen.2015.04.003

Keykavoos R, Mankidy R, Ma H, Jones P, Soltan J (2013) Mineralization of bisphenol A by catalytic ozonation over alumina. Sep Purif Technol 107:310–317. https://doi.org/10.1016/j.seppur.2013.01.050

Kim JK, Kim SS, Kim WJ (2005) Sol-gel synthesis and properties of multiferroic $BiFeO_3$. Mater Lett 59:4006–4009. https://doi.org/10.1016/j.matlet.2005.07.050

Konstantinou IK, Albanis TA (2004) TiO_2-assisted photocatalytic degradation of azo dyes in aqueous solution: kinetic and mechanistic investigations. Appl Catal B Environ 49:1–14. https://doi.org/10.1016/j.apcatb.2003.11.010

Kumar SG, Rao KSRK (2015) Tungsten-based nanomaterials (WO_3 & Bi_2WO_6): modifications related to charge carrier transfer mechanisms and photocatalytic applications. Appl Surf Sci 355:939–958. https://doi.org/10.1016/j.apsusc.2015.07.003

Kumar SG, Rao KSRK (2017) Comparison of modification strategies towards enhanced charge carrier separation and photocatalytic degradation activity of metal oxide semiconductors (TiO2, WO3 and ZnO). Appl Surf Sci 391:124–148. https://doi.org/10.1016/j.apsusc.2016.07.081

Lam SM, Sin JC, Mohamed AR (2017) A newly emerging visible light-responsive $BiFeO_3$ perovskite for photocatalytic applications: a mini review. Mater Res Bull 90:15–30. https://doi.org/10.1016/j.materresbull.2016.12.052

Li D, Zhou Z, Qing D, He Y, Wu T, Miao M, Wang J, Weng X, Ferber JR, Herrinton LJ, Zhu Q, Gao E, Checkoway H, Yuan W (2010) Occupational exposure to bisphenol-A (BPA) and the risk of self-reported male sexual dysfunction. Hum Reprod 25:519–527. https://doi.org/10.1093/humrep/dep381

Li J, Zhao W, Guo Y, Wei Z, Han M, He H, Yang S, Sun C (2015) Facile synthesis and high activity of novel $BiVO_4/FeVO_4$ heterojunction photocatalyst for degradation of metronidazole. Appl Surf Sci 351:270–279. https://doi.org/10.1016/j.apsusc.2015.05.134

Lin X, Lv P, Quan Q, Li H, Zhai H, Liu C (2012) Bismuth titanate microspheres: directed synthesis and their visible light photocatalytic activity. Appl Surf Sci 258:7146–7153. https://doi.org/10.1016/j.apsusc.2012.04.019

Liu Y, Ding Z, Lv H, Guang J, Li S, Jiang J (2015) Hydrothermal synthesis of hierarchical flower-like Bi_2WO_6 microspheres with enhanced visible-light photoactivity. Mater Lett 157:158–162. https://doi.org/10.1016/j.matlet.2015.05.024

Majid F, Mirza ST, Riaz S, Naseem S (2015) Sol-Gel synthesis of $BiFeO_3$ nanoparticles. Mater Today Proc 2:5293–5297. https://doi.org/10.1016/j.matpr.2015.11.038

Manfo FP, Jubendradass R, Nantia EA, Moundipa PF, Mathur PP (2014) Adverse effects of bisphenol A on male reproductive function. Rev Environ Contam Toxicol 228:57–82. https://doi.org/10.1007/978-3-319-01619-1_3

Paulose T, Speroni L, Sonnenschein C, Soto AM (2015) Estrogens in the wrong place at the wrong time: fetal BPA exposure

and mammary cancer. Reprod Toxicol 54:58–65. https://doi.org/10.1016/j.reprotox.2014.09.012

Puangpetch T, Sommakettarin P, Chavadej S, Sreethawong T (2010) Hydrogen production from water splitting over Eosin Y-sensitized mesoporous-assembled perovskite titanate nanocrystal photocatalysts under visible light irradiation. Int J Hydrogen Energy 35:12428–12442. https://doi.org/10.1016/j.ijhydene.2010.08.138

Son LT, Takaomi K (2011) Hollow-fiber membrane absorbents embedded molecularly imprinted polymeric spheres for bisphenol A target. J Membr Sci 384:117–125. https://doi.org/10.1016/j.memsci.2011.09.013

Sood S, Umar A, Mehta SK, Kansal SK (2015) α-Bi_2O_3 nanorods: an efficient sunlight active photocatalyst for degradation of Rhodamine B and 2,4,6-trichlorophenol. Ceram Int 41:3355–3364. https://doi.org/10.1016/j.ceramint.2014.10.038

Sun B, Zhou G, Gao T, Zhang H, Yu H (2016) NiO nanosheet/TiO_2 nanorod-constructed p–n heterostructures for improved photocatalytic activity. Appl Surf Sci 364:322–331. https://doi.org/10.1016/j.apsusc.2015.12.158

Takamiya M, Magan N, Warner PJ (2008) Impact assessment of bisphenol A on lignin-modifying enzymes by basidiomycete Trametes versicolor. J Hazard Mater 154:33–37. https://doi.org/10.1016/j.jhazmat.2007.09.098

Tong T, Zhang H, Chen J, Jin D, Cheng J (2016) The photocatalysis of $BiFeO_3$ disks under visible light irradiation. Catal Comm 87:23–26. https://doi.org/10.1016/j.catcom.2016.08.030

Vom Saal FS, Welshons WV (2014) Evidence that bisphenol A (BPA) can be accurately measured without contamination in human serum and urine, and that BPA causes numerous hazards from multiple routes of exposure. Mol Cell Endocrinol 398:101–113. https://doi.org/10.1016/j.mce.2014.09.028

Xiao X, Hu R, Liu C, Xing C, Qian C, Zuo X, Nan J, Wang L (2013) Facile large-scale synthesis of β-Bi_2O_3 nanospheres as a highly efficient photocatalyst for the degradation of acetaminophen under visible light irradiation. Appl Catal B: Environ 140–141:433–443. https://doi.org/10.1016/j.apcatb.2013.04.037

Yan Y, Zhou Z, Cheng Y, Qiu L, Gao C, Zhou J (2014a) Template-free fabrication of α- and β-Bi_2O_3 hollow spheres and their visible light photocatalytic activity for water purification. J Alloys Compd 605:102–108. https://doi.org/10.1016/j.jallcom.2014.03.111

Yan Y, Zhou Z, Zhao X, Zhou J (2014b) A controlled anion exchange strategy to synthesize core-shell beta-bismuth oxide/bismuth sulfide hollow heterostructures with enhanced visible-light photocatalytic activity. J Colloid Interface Sci 435:91–98. https://doi.org/10.1016/j.jcis.2014.08.027

Yap PS, Lim TT, Lim M, Srinivasan M (2010) Synthesis and characterization of nitrogen-doped TiO_2/AC composite for the adsorption–photocatalytic degradation of aqueous bisphenol-A using solar light. Catal Today 151:8–13. https://doi.org/10.1016/j.cattod.2010.01.012